Materials Science & Engineering A 697 (2017) 233–237

Contents lists available at ScienceDirect

Materials Science & Engineering A

journal homepage: www.elsevier.com/locate/msea

Strain-field evolution in a CuZr-based bulk metallic glass composite during tensile deformation

Zhiliang Ning[a,b,*], Weizhong Liang[c,**], Zhijie Kang[c], Haichao Sun[a,b], Jianfei Sun[a,b]

[a] School of Materials Science and Engineering, Harbin Institute of Technology, Harbin 150001, People's Republic of China
[b] National Key Laboratory for Precision Hot Processing of Metals, Harbin Institute of Technology, Harbin 150001, People's Republic of China
[c] School of Materials Science and Engineering, Heilongjiang University of Science and Technology, Harbin 150022, People's Republic of China

ARTICLE INFO

Keywords:
Digital image correlation technique
Bulk metallic glass composite
Strain heterogeneity
Plastic deformation

ABSTRACT

Bulk metallic glass composites (BMGCs) reinforced with a B2-CuZr phase exhibit improved ductility. However, the relationship between the macroscopic plastic deformation of BMGCs and the microscopic strain evolution is still poorly understood. Here, we investigated the strain-field evolution of a $Cu_{44.3}Zr_{48}Al_4Nb_{3.7}$ (at%) BMGC by using an in-situ digital image correlation technique during tensile deformation. The strain-field evolution in the composite containing B2-CuZr particles was analysed and compared to that in a $Cu_{47}Zr_{48}Al_4Nb_1$ BMG. We found that a high degree of shear strain heterogeneity played a key role in the macroscale plastic deformation, which was attributed to the intrinsic structural heterogeneities. These findings have implications for the development of BMGCs with excellent tensile properties.

1. Introduction

Extensive efforts have been devoted to improving room-temperature plasticity of bulk metallic glasses (BMGs) and then enable them to be used as structural materials [1–6]. In particular, BMG-matrix composites (BMGCs) have been developed to overcome the limited ductility in BMGs through introducing a ductile crystalline phase into the glassy-phase matrix [7–12]. In the research on these composites, a CuZr-based BMGC containing a uniform distribution of a single B2-CuZr phase was successfully developed [13–17]. The martensitic phase transformation mediated plasticity of the B2-CuZr phase was a key factor contributing to the tensile ductility of CuZr-based BMGCs [18,19]. Macroscopically, the plastic deformations of BMGCs manifest as serrated flows in the stress-strain curves [20], during which the strain energy accumulated in the elastic deformation regime can be released in this plastic stage and the final fracture process. Microscopically, locally structural heterogeneities, such as the interfaces between glassy matrix and crystals , free volume regions , or shear transformation zones, strongly influence the formation and evolution of shear bands, and affect the strain energy transport pathway, which then govern the macroscopic plastic deformation behaviour [20]. These heterogeneities can perturb the strain energy distribution during the plastic strain regime. However, the relationship between the macroscopic plastic deformation of BMGCs and microscopic strain energy distribution is still not well understood.

Digital image correlation (DIC) technique is an effective method for observing the strain-field evolution with stress through sequentially recording the digital maps of surface features on the tested sample during deformation, followed by pattern-matching algorithm based on post-processing of these images [20–23]. The DIC technique has been widely used in the investigation of BMGs [20,24,25]. The strain concentration and the critical strain value for the operation of shear banding in BMGs can be quantitatively evaluated on the basis of DIC observations. For BMGCs, the second phase embedded into the glassy phase should perturb the shear-banding behaviour. Accordingly, the strain field before shear banding should be changed by the second phase in BMGCs. However, to date, the strain concentration during the deformation of BMGCs has not been paid attention. Therefore, in this study, we investigated the relationships among microscopic strain, strain energy accumulation and serrated flow in a $Cu_{44.3}Zr_{48}Al_4Nb_{3.7}$ (at%) BMGC under different tensile deformation stages through in-situ observations by the DIC technique. The macroscopic plastic deformation mechanism in BMGCs was discussed.

2. Experimental

Ingots of $Cu_{48-x}Zr_{48}Al_4Nb_x$ (x = 1, 3.7 at%, denoted as 1Nb and 3.7Nb, respectively) alloys were prepared by arc melting the pure elements in a Ti-gettered argon atmosphere. Cylindrical rods with a

* Corresponding author at: School of Materials Science and Engineering, Harbin Institute of Technology, Harbin 150001, People's Republic of China.
** Corresponding author at: School of Materials Science and Engineering, Heilongjiang University of Science and Technology, Harbin 150022, People's Republic of China.
E-mail addresses: zhiliangning@sina.com (Z. Ning), wzliang1966@126.com (W. Liang).

http://dx.doi.org/10.1016/j.msea.2017.05.020
Received 28 December 2016; Received in revised form 9 April 2017; Accepted 4 May 2017
Available online 08 May 2017
0921-5093/ © 2017 Elsevier B.V. All rights reserved.

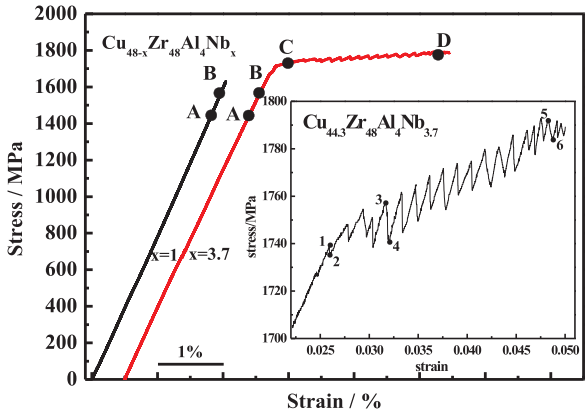

Fig. 1. Tensile stress-strain curves of 1Nb and 3.7Nb samples. The inset shows a magnified region of the tensile stress-strain curve of the 3.7Nb sample.

diameter and length of 3 and 47 mm, respectively, were drop-cast into a copper mould. The microstructures of the 1Nb and 3.7Nb alloys were investigated in our previous work, which revealed that the 1Nb alloy was fully glassy phase and that the 3.7Nb alloy was a BMGC consisting of a B2-CuZr phase and a glassy matrix [26]. For the tensile test, dog-bone-shaped samples with a gauge dimension of 10 mm × 2 mm × 1 mm were cut from the cast rods. Prior to tension, the tensile specimens were spray-painted to generate an artificial speckle suitable for the DIC measurement (shown in Figs. 2 and 3a). Uniaxial tension tests were performed at an initial strain rate of $3.5\times10^{-4}\ s^{-1}$ using an INSTRON-5569 testing machine at room temperature. The spray-painted sample surface was illuminated by two fibre-optic white-light sources during loading. A CCD video camera (JAI CV-AI) with a resolution of 5 μm/pixel was used to capture the consecutive speckle images at a frequency of 4 Hz during the deformation. A rectangular 420 × 140 pixel frame located at the centre of the sample surface was selected for strain calculations. The sequential speckle images were calculated using the Newton-Raphson iteration algorithm, and the strain distributions at different loads could be identified by a series of pronounced contour maps.

3. Results and discussion

The in-situ tension stress-strain curves of $Cu_{48-x}Zr_{48}Al_4Nb_x$ (x = 1, 3.7 at%) samples are plotted in Fig. 1. The 1Nb sample shows a slightly yielding plasticity after elastic deformation without an obviously plastic flow. The stress-strain curve of the 3.7Nb sample explicitly reveals a significantly macroscopic plastic deformation regime composed of a series of serrated events, as shown in the inset. The serrated events in the 3.7Nb sample suggest that the stress fluctuation in the plastic regime might be related to microscopic strain distribution.

Fig. 2a-c present the surface speckle image without loading and the DIC results of the in-situ tension of the 3.7Nb sample. The normal strain (ε_y, along the loading direction) fields, and the shear strain (γ_{xy}) fields recorded at different stresses indicated by the numbers in the inset of Fig. 1, are mapped in Figs. 2b and c, respectively. It can be seen that the stress approaching the yield strength of 1738 MPa (at point 1) causes the strain fields to distribute inhomogeneously. Especially, the strain-concentration striations are formed in the ε_y field, and some strain-concentration regions emerge in the γ_{xy} field, in which the maximum ε_y and γ_{xy} values reach 0.045 and −0.014, respectively. Slightly decreasing the stress to 1736 MPa (at point 2) does not significantly influence the evolution of strain fields. From points 2–3, more strain-concentration striations are observed as compared to the case at point 2 in the ε_y field. In the γ_{xy} field, the area of the positive strain-concentration region is increased with increasing the strain from points 2–3. When the stress decreases from 1757 MPa to 1741 MPa (from points 3–4), the strain-concentration striations in the ε_y field and the positive strain-concentration regions in the γ_{xy} field are enlarged. With increasing plastic strain, the negative strain-concentration regions in the γ_{xy} fields is enhanced, which can be observed from points 4–6. Meantime, the maximum strain value and the area of the striation in the ε_y field are enlarged from points 4–6. The strain-concentration striation in the ε_y field is corresponding to the region of the negative strain-concentration in the γ_{xy} field. The negative strain-concentration regions, and the positive strain-concentration regions are formed simultaneously in the γ_{xy} field during the tension, indicating the unique microscopic strain feature of the BMGC.

Fig. 3a-c show the surface speckle image without loading and the DIC results for the in- situ tension test of the 1Nb sample. The normal strain (ε_y) fields and the shear strain (γ_{xy}) fields at different stresses are

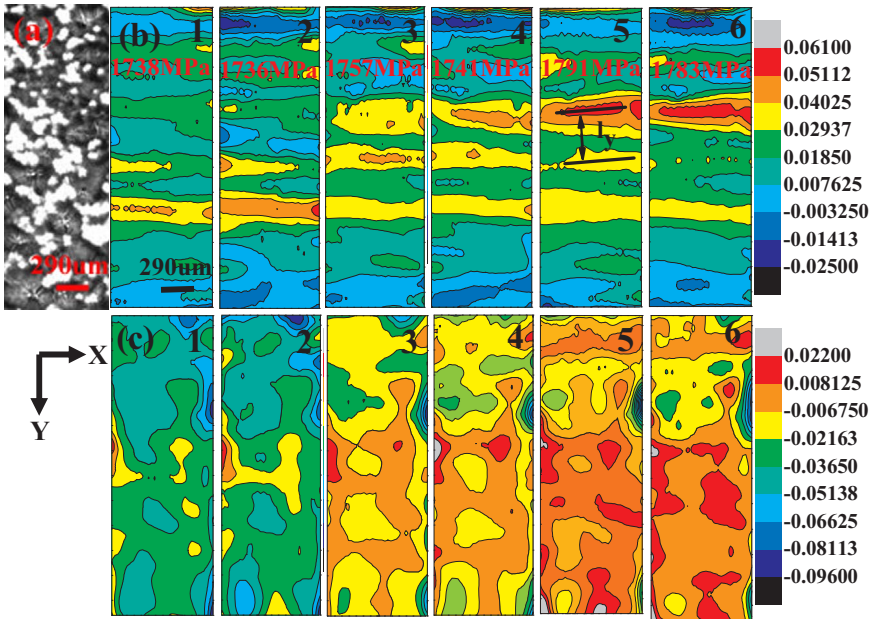

Fig. 2. In-situ tension DIC images of 3.7Nb BMGC sample. (a) Surface speckle image without loading. (b) Contour maps of the ε_y field, (c) Contour maps of the γ_{xy} field, image numbers correspond to these marked in the inset in Fig. 1.

Download English Version:

https://daneshyari.com/en/article/5455771

Download Persian Version:

https://daneshyari.com/article/5455771

Daneshyari.com